Formation of gold–silver sulfides and native gold in Fe–Ag–Au–S system

G.A. Pal'yanova [a,*], K.A. Kokh [a], Yu.V. Seryotkin [a,b]

[a] *V.S. Sobolev Institute of Geology and Mineralogy, Siberian Branch of the Russian Academy of Sciences,
pr. Akademika Koptyuga 3, Novosibirsk, 630090, Russia*
[b] *Novosibirsk State University, ul. Pirogova 2, Novosibirsk, 630090, Russia*

Abstract

We carried out experiments on crystallization of Fe-containing melts $FeS_2Ag_{0.1-0.1x}Au_{0.1x}$ (x = 0.05, 0.2, 0.4, and 0.8) with Ag/Au weight ratios from 10 to 0.1. Mixtures prepared from elements in corresponding proportions were heated in evacuated quartz ampoules to 1050 ℃ and kept at this temperature for 12 h; then they were cooled to 150 ℃, annealed for 30 days, and cooled to room temperature. The solid-phase products were studied by optical and electron microscopy and X-ray spectroscopy. The crystallization products were mainly from iron sulfides: monoclinic pyrrhotite ($Fe_{0.47}S_{0.53}$ or Fe_7S_8) and pyrite ($Fe_{0.99}S_{2.01}$). Gold–silver sulfides (low-temperature modifications) are present in all synthesized samples. Depending on Ag/Au, the following sulfides are produced: acanthite (Ag/Au = 10), solid solutions $Ag_{2-x}Au_xS$ (Ag/Au = 10, 2), uytenbogaardtite (Ag/Au = 2, 0.75), and petrovskaite (Ag/Au = 0.75, 0.12). They contain iron impurities (up to 3.3 wt.%). Xenomorphic micro- (<1–5 µm) and macrograins (5–50 µm) of Au–Ag sulfides are localized in pyrite or between the grains of pyrite and pyrrhotite. High-fineness gold was detected in the samples with initial ratio Ag/Au ≤ 2. It is present as fine and large rounded microinclusions or as intergrowths with Au–Ag sulfides in pyrite or, more seldom, at the boundary of pyrite and pyrrhotite grains. This gold contains up to 5.7 wt.% Fe. Based on the sample textures and phase relations, a sequence of their crystallization was determined. At ~1050 ℃, there are probably iron sulfide melt L_1 (Fe,S ≫ Ag,Au), gold–silver sulfide melt L_2 (Au,Ag,S ≫ Fe), and liquid sulfur L_S. On cooling, melt L_1 produces pyrrhotite; further cooling leads to the crystallization of high-fineness gold (macrograins from L_1 and micrograins from L_2) and Au–Ag sulfides (micrograins from L_1 and macrograins from L_2). Pyrite crystallizes after gold–silver sulfides by the peritectic reaction $FeS + L_S = FeS_2$ at ~743 ℃. Elemental sulfur is the last to crystallize. Gold–silver sulfides are stable and dominate over native gold and silver, especially in pyrite-containing ores with high Ag/Au ratios.

© 2012, V.S. Sobolev IGM, Siberian Branch of the RAS. Published by Elsevier B.V. All rights reserved.

Keywords: Fe–Ag–Au–S system; iron sulfide melt; pyrite; pyrrhotite; gold–silver sulfide melt; solid solutions $Ag_{2-x}Au_xS$; uytenbogaardtite; petrovskaite; high-fineness gold

Introduction

Gold–silver sulfides, uytenbogaardtite (Au_3AuS_2) and petrovskaite (AgAuS), were revealed in sulfide ores of many deposits and ore occurrences (Barton et al., 1978; Castor and Sjoberg, 1993; Nesterenko et al., 1984; Savva and Pal'yanova, 2007). The size of their grains varies from submicron (<0.1 µm) to few centimeters; most often, it is fractions of millimeter. Several physicochemical models for the genesis of gold–silver sulfides were elaborated. They were tentatively called hypogene (hydrothermal and paleosolfataric) (Pal'yanova and Savva, 2009; Pal'yanova et al., 2011c; Savva et al., 2010a;) and hypergene (Pal'yanova and Savva, 2007; Savva and Pal'yanova, 2007; Savva et al., 2010b). However, they might also form from sulfide melts $Ag_{2-x}Au_xS$ (0 < x < 1.7) (Barton, 1980; Palyanova et al., 2011a,b). Gold–silver sulfides $(Au,Ag,Fe)_2S$ were discovered together with iron, copper, and nickel sulfides in carbonaceous chondrites (Geiger and Bischoff, 1995). Uytenbogaardtite grown over electrum was found in the ijolites and nepheline syenites of the Goryachaya Gora massif (Sazonov et al., 2008). In the ores from the Original Bullford deposit in Canada (Castor and Sjoberg, 1993), exsolution structures were discovered, which are myrmekite-like intergrowths of native gold and uytenbogaardtite. Not only argentite (acanthite) but also uytenbogaardtite were recognized in the ores from deposits in the Noril'sk district (Sluzhenikin and Mokhov, 2002, 2010; Spiridonov, 2010a,b). A high extracting capacity of Fe-containing sulfide melts for Au and Ag was reported by Barnes et al. (2006), Czamanske et al. (1992), Mungall et al. (2005), Nadeau et al., 2010; Ryabchikov et al. (1999), Wager and Brown (1968). The goal

---

* Corresponding author.
E-mail address: palyan@igm.nsc.ru (G.A. Pal'yanova)

of this work was to study the behavior of gold and silver during the crystallization of high-temperature Fe–Ag–Au–S melts and to estimate the formation conditions of Au–Ag sulfides and native gold. Study of the behavior of Au and Ag in Fe- and S-containing systems is of interest for revealing their primary state in iron sulfides. We hope the performed work will help to locate gold–silver sulfides (uytenbogaardtite and perovskaite) in sulfide-containing ores. The system Fe–Ag–Au–S has a simplified composition as compared with the natural ones and is an intermediate link between simple and complex magmatic systems containing Cu, Ni, and other elements.

Experimental conditions of synthesis

We studied the behavior of gold and silver during the crystallization of melts in the system Fe–Au–Ag–S with a constant atomic S/Fe ratio equal to 2 and the total content of noble metals (Au + Ag) not exceeding 10 wt.% of the total content of major elements (Fe + S). The contents of Au and Ag were higher than their maximum possible contents in iron sulfides (Chareev, 2006; Cook and Chryssoulis, 1990; Mironov et al., 1987; Tauson et al., 1996, 1998, 2005), which favored the formation of their individual mineral phases in the system under study. The contents of noble metals in the experiments were specified in different proportions to elucidate the influence of Ag/Au on the composition of Au–Ag minerals. The studied system Fe–Au–Ag–S can be formally described as 1 mole FeS_2 + 0.1 mole $Ag_{1-x}Au_x$, or $FeS_2 \cdot Ag_{0.1-0.1x}Au_{0.1x}$, where the x values (mole fraction of gold in Au–Ag alloy) was specified equal to 0.05, 0.2, 0.4, and 0.8, which corresponded to atomic ratios from 19 to 0.25 and weight Ag/Au ratios of 10.4 to 0.14. Hereafter, we use rounded values of weight Ag/Au ratios—10, 2, 0.8, and 0.1.

As starting materials for the experiments, we used gold and silver (99.99%) as well as iron and sulfur (special-purity grade) (Table 1). The total sample weights were ~500 mg; the accuracy of weighing was ±0.05 mg. The starting materials were placed into quartz ampoules with a quartz rod to minimize the free volume. The ampoules were sealed at a residual pressure of ~10^{-2} torr. The samples were heated to 1050 ℃ for three days, were kept at this temperature for 12 h, and then were cooled to 150 ℃ with a rate of 0.2 ℃/min and annealed at this temperature for 30 days. Afterwards, the furnace was switched off and cooled to room temperature for ~7 h.

The Fe–S diagram (Fig. 1, a) shows the stability domains of phases in the temperature range 0–1200 ℃ (Waldner and Pelton, 2005). The black point (Fig. 1, a) corresponds to the atomic S/Fe ratio (33.33 at.% Fe, 66.66 at.% S) during the experiments and the maximum temperature of the ampoule heating (~1050 ℃). The atomic ratio (Fe + Ag + Au)/S was 1.8, which is lower than Fe/S in pyrite but higher than Fe/S in pyrrhotite. Figure 1, b shows the system Ag–Au–S with phases stable at room temperature (Barton, 1980; Osadchii and Rappo, 2004; Vol and Kogan, 1976). The points correspond to the initial Ag/Au ratios in the system, with S and Fe being ignored. We omit the Ag_2S–Au_2S section reflecting the phase relations over a wide temperature range (Barton, 1980), because it is identical to that in Fig. 1 in our recent paper concerned with the system Ag–Au–S (Pal'yanova et al., 2011b).

The annealing was performed at 150 ℃, which is lower than the temperature of phase transitions of Au–Ag sulfides ($\alpha \leftrightarrow \beta$ at 307 ℃ for petrovskaite, at 187 ℃ for uytenbogaardtite, and at 177 ℃ for acanthite). This temperature was chosen in order to obtain a crystalline structure of low-temperature polymorphic petrovskaite and uytenbogaardtite.
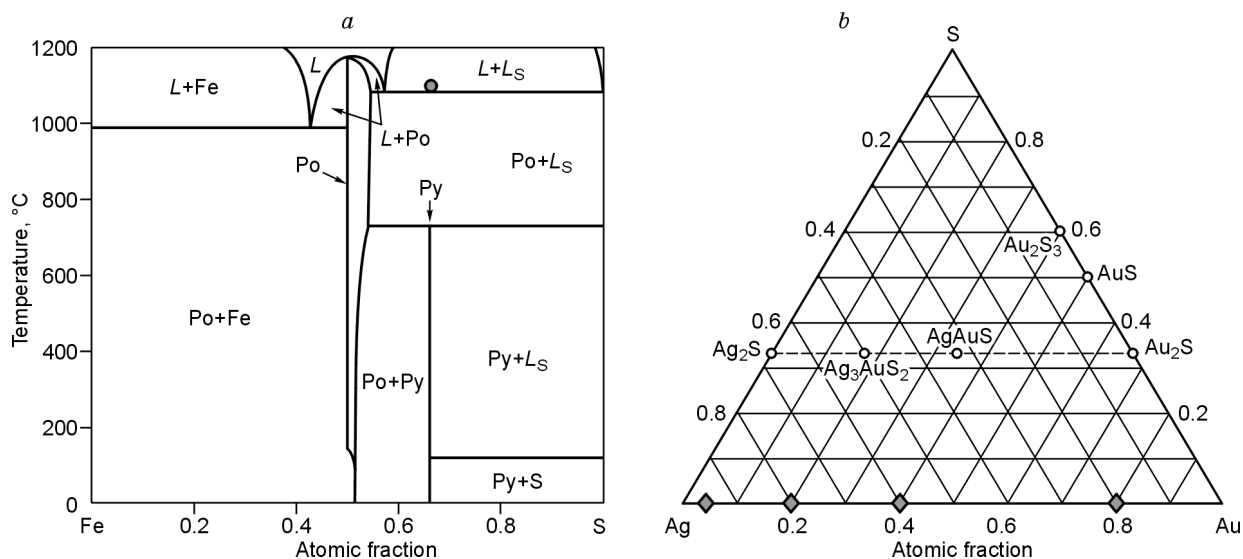

Fig. 1. Diagrams of phase stability in the system Fe–S (Waldner and Pelton, 2005) in the temperature range 0–1200 ℃ (a) and compositions of phases stable in the system Au–Ag–S at room temperature (Barton, 1980; Osadchii and Rappo, 2004; Vol and Kogan, 1976) (b). L, melt; L_S, liquid sulfur; Po, pyrrhotite; Py, pyrite. Black point corresponds to initial atomic Fe/S ratios in the experiments and the maximum temperature of ampoule heating (a). Rhombuses mark initial atomic Au/Ag ratios (b).

Table 1. Results of X-ray spectral microprobe analysis of solid phases in experiments with initial compositions FeS$_2$Ag$_{0.1-0.1x}$Au$_{0.1x}$ ($x = 0.05$–0.8)

Experiment	Initial composition of system, solid phases	Contents of elements in initial system and solid phases					
		Ag	Au	Fe	S	Σ	Initial Ag/Au weight ratios and formular units of solid phases
1	$x = 0.05$	**31.94**	**3.2**	**111.4**	**128.2**	**274.74**	Ag/Au = 10
	Pyrrhotite	*0*	*0*	*59.98*	*38.85*	*98.83*	Fe$_{0.4}$7S$_{0.53}$
		0	0	46.99	53.01	100.00	
	Pyrite	*0*	*0*	*46.89*	*54.73*	*101.62*	Fe$_{0.99}$S$_{2.01}$
		0	0	32.97	67.03	100.00	
	(Ag,Au,Fe)$_2$S	*79.00*	*15.10*	*1.9*	*14.05*	*99.65*	Ag$_{1.6}$Au$_{0.2}$Fe$_{0.1}$S$_{1.1}$
		53.17	6.47	2.87	36.99	100.00	
	Acanthite	*90.2*	*0*	*0*	*11.15*	*101.35*	Ag$_2$S
		70.64	0	0	29.36	100.00	
2	$x = 0.2$	**24.5**	**11.2**	**111.4**	**128.4**	**275.5**	Ag/Au = 2
	Pyrrhotite	*0*	*0*	*60.74*	*39.22*	*99.96*	Fe$_{0.4}$7S$_{0.53}$
		0	0	47.06	52.94	100.00	
	Pyrite	*0*	*0*	*47.45*	*54.09*	*101.54*	Fe$_{1.00}$S$_{2.00}$
		0	0	33.49	66.51	100.00	
	Uytenbogaardtite	*55.41*	*29.2*	*1.09*	*11.69*	*97.39*	Ag$_{2.9}$Au$_{0.9}$Fe$_{0.1}$S$_{2.1}$
		49.11	14.17	1.87	34.86	100.00	
	(Ag,Au,Fe)$_2$S	*51.59*	*34.64*	*0.94*	*14.68*	*101.84*	Ag$_{1.3}$Au$_{0.5}$Fe$_{0.1}$S$_{1.2}$
		42.37	15.58	1.49	40.56	100.00	
	Au–Ag–Fe alloy	*14.62*	*75.07*	*5.72*	*0*	*95.41*	Au$_{0.62}$Ag$_{0.22}$Fe$_{0.16}$ (N_{Au} = 750‰)
		21.89	61.56	16.54	0	100.00	
3	$x = 0.4$	**16.3**	**20.0**	**111.0**	**128.4**	**275.7**	Ag/Au = 0.8
	Pyrrhotite	*0*	*0*	*59.65*	*38.96*	*98.61*	Fe$_{0.47}$S$_{0.53}$
		0	0	46.78	53.22	100.00	
	Pyrite	*0*	*0*	*46.34*	*53.68*	*100.02*	FeS$_2$
		0	0	33.14	66.86	100.00	
	Petrovskaite	*31.69*	*57.1*	*0.91*	*12.58*	*102.28*	AgAuS
		29.6	29.21	1.64	39.54	100.00	
	Uytenbogaardtite	*55.07*	*31.72*	*2.15*	*12.83*	*101.77*	Ag$_{2.8}$Au$_{0.9}$Fe$_{0.1}$S$_{2.1}$
		45.98	14.5	3.47	36.04	100.00	
	Au–Ag–Fe alloy	*5.58*	*96.77*	*1.39*	*0*	*103.74*	Au$_{0.87}$Ag$_{0.09}$Fe$_{0.04}$ (N_{Au} = 930‰)
		9.11	86.51	4.38	0	100.00	
4	$x = 0.8$	**4.4**	**32.7**	**111.2**	**128.3**	**276.6**	Ag/Au = 0.1
	Pyrrhotite	*0*	*0*	*61.98*	*40.11*	*102.09*	Fe$_{0.47}$S$_{0.53}$
		0	0	47.01	52.99	100.00	
	Pyrite	*0*	*0*	*46.18*	*52.36*	*98.54*	FeS$_2$
		0	0	33.61	66.39	100.00	
	Petrovskaite	*27.94*	*56.61*	*3.32*	*13.49*	*101.37*	AgAuS
		28.52	29.87	3.84	37.77	100.00	
	Au–Ag–Fe alloy	*5.36*	*92.07*	*2.51*	*0*	*99.94*	Au$_{0.83}$Ag$_{0.09}$Fe$_{0.08}$ (N_{Au} = 920‰)
		8.84	83.16	8	0	100.00	

Note. Bold figures, mg; italic figures, wt.%; normal figures, at.%. Contents in % and in molar fractions are one unit higher than the significant values.

Moreover, since the experiments in the system Fe–Ag–Au–S were performed in the same temperature regime as the experiments in the system Ag–Au–S (Pal'yanova et al., 2011a,b), we could compare their results and elucidate the role of iron sulfides and sulfur in the formation of Au–Ag sulfides as well as native gold.

To determine the optimal duration of the annealing by the example of the system Au–Ag–S, we carried out a series of kinetic experiments with $Ag_{1.6}Au_{0.4}S$ for 7, 14, 32, and 130 days and an experiment without annealing. The number, composition, and structure of synthesized phases did not change when the annealing was performed for 14 days and more. The samples obtained without annealing and after annealing for seven days had an inhomogeneous composition (data of microprobe analysis) and contained additional phases similar in composition to the initial sample $Ag_{1.6}Au_{0.4}S$ (Pal'yanova et al., 2011b).

Polished sections were prepared from 1/3 of each sample. The synthesized solid-phase products were studied by optical and electron microscopy. The chemical composition of phases was determined on a JSM-6510LV (JEOL Ltd) electron scanning microscope with an INCA Energy 350 Oxford Instruments Analytical energy dispersion spectrometer at the Institute of Geology and Mineralogy, Novosibirsk. Operation conditions: accelerating voltage—20 kV, probe current—1 nA,

spectrum recording during analysis—15 s, spectrum recording during X-ray radiation—up to 3000 s. As reference samples, we used Au–Ag alloy (750‰) for Au and Ag analysis and $CuFeS_2$ for S and Fe analysis. To eliminate the presence of background amounts of elements from the surrounding phases, we examined only large grains (>10 μm). The accuracy of X-ray microprobe analysis was 1.5 rel.% for Au, 1 rel.% for Fe and Ag, and 0.5 rel.% for S. The detection limit of Au and Ag present as impurities in iron sulfides is 0.6 wt.%.

An X-ray phase analysis of the synthesized phases was carried out using an ARL X'TRA Thermo Scientific X-ray powder diffractometer with a Peltier-cooled solid Si-Li detector. Diffraction data were collected in the 2θ range of 5º–60º with a 0.02º step and the collection time of 10 s. The results were treated using the WinXRD 2.0-6 (Thermo Scientific) program. For phase analysis, the PDF-4 Minerals database (The Powder Diffraction..., 2006) was used.

Results of investigation of synthesized solid phases

Table 1 lists the compositions of the synthesized solid phases. Note that the main phases in all experiments are iron sulfides (Figs. 2–5): pyrrhotite ($Fe_{0.47}S_{0.53}$ or Fe_7S_8) and pyrite (FeS_2). The inequigranular texture of the synthesized
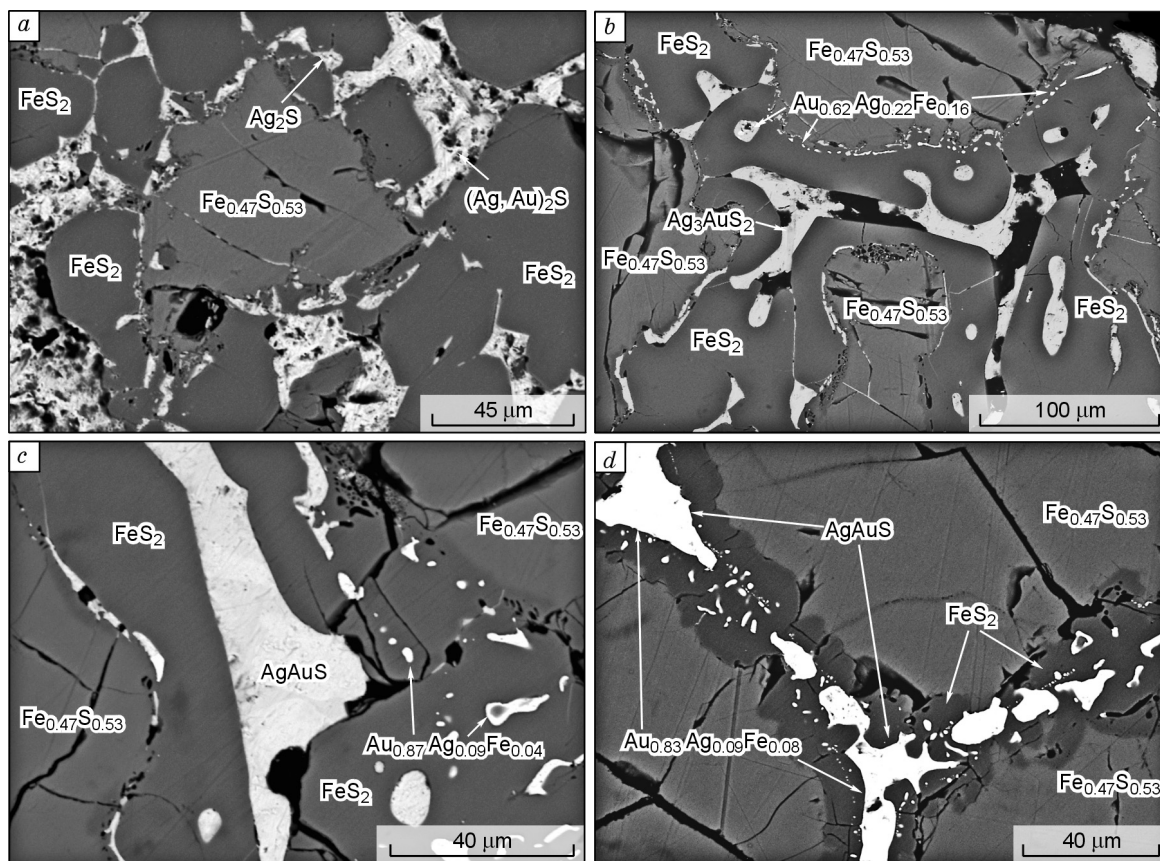

Fig. 2. Reflected-electron images of large and fine grains of Au–Ag sulfides and native gold localized in pyrite and interstices of iron sulfides in experiments with different initial Ag/Au ratios: a, 10; b, 2; c, 0.8; d, 0.1.
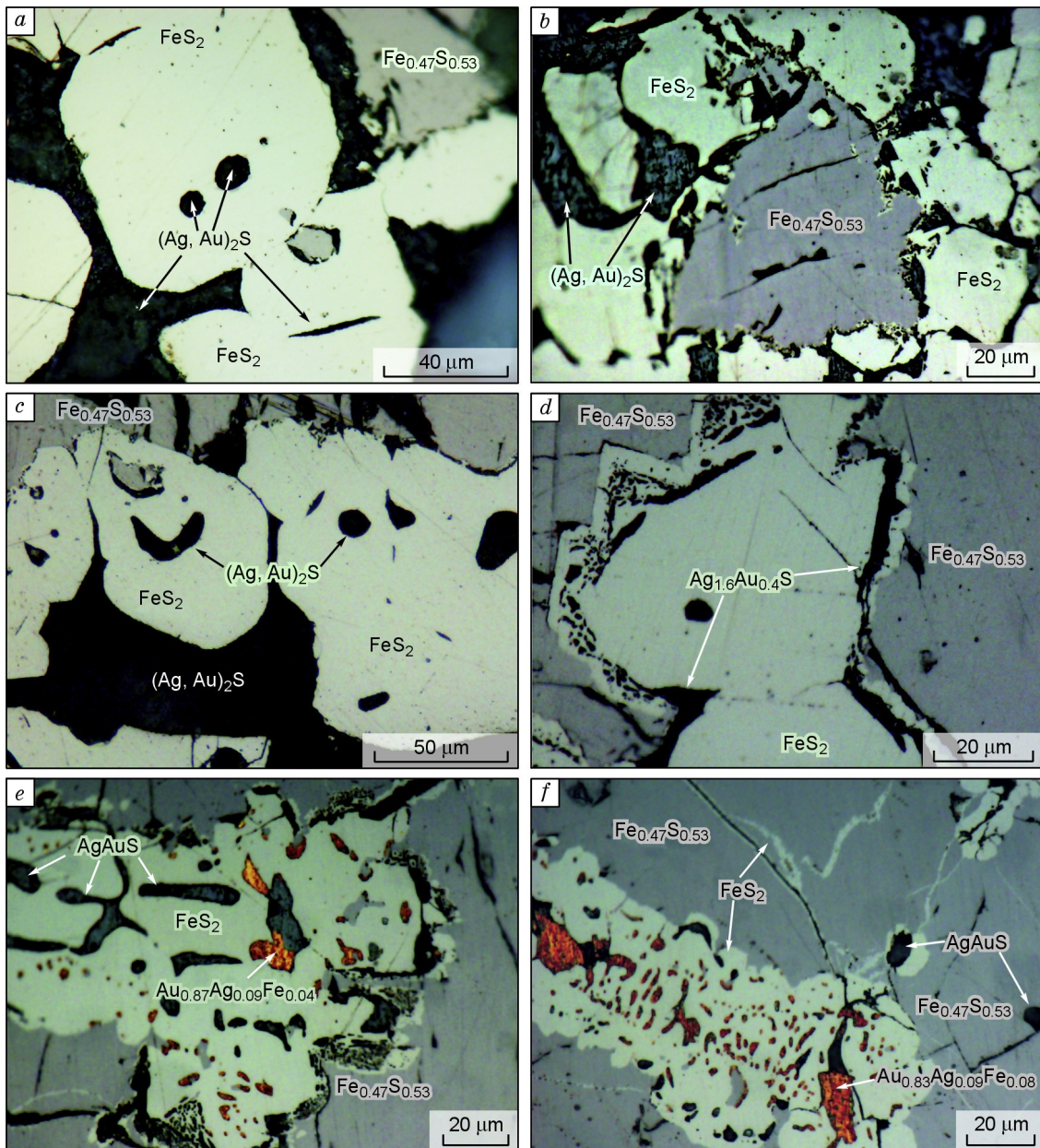
Fig. 3. Reflected-light photos (Olympus BX51 optical microscope) of xenomorphic gold–silver sulfide grains in pyrite and emulsion phenocrysts of native gold and Au–Ag sulfides in its core and rim, which are localized parallel to the pyrite–pyrrhotite boundary: a, b, Ag/Au = 10; c, d, 2; e, 0.8; f, 0.1.

samples is well seen in Figs. 2, a–d, 3, b–f, and Fig. 5, a, b. Pyrrhotite has large euhedral grains with fine-grained aggregates of pyrite and Au–Ag sulfides (Figs. 2, a and 3, b) and alloys (Figs. 2, b–d and 3, c–f) in the interstices. The pyrrhotite–pyrite boundary is resorbed and is obviously corroded (Figs. 2, a–d and 3, b–f). The pyrrhotite grains reach 300 μm in size; pyrite, 100 μm; and Au–Ag sulfides, 50 μm. The pyrite grains are euhedral. Locally, the pyrite bears fine pyrrhotite inclusions of irregular shape (Fig. 3, a). It also fills thin cracks in the pyrrhotite (Fig. 3, e, f). Aggregates of iron sulfide microcrystals have been revealed on the sample surface (Fig. 4, a–f). The pyrite occurs as cuboctahedral crystals (Fig. 4, b), and the pyrrhotite, as pseudohexagonal pyramids or prisms (Fig. 4, c, d). Note that the pyrrhotite lacks gold

and silver microimpurities, or their content is below their detection limit in X-ray microprobe analysis.

The Au–Ag sulfide grains are xenomorphic and are arranged between the pyrite grains or between the pyrite and pyrrhotite grains (Figs. 2, a–d, 3, a–f, 4, a–f, and 5, a, b). Moreover, Au–Ag sulfides as rounded grains or intergrowths with Au–Ag melts form emulsion-like impregnations in pyrite (Figs. 2, a–d, 3, a–f, 4, a–f). Gold–silver alloys were detected only in experiments 2–4 (Ag/Au ≤ 2) (Table 1). The content and size of the alloy grains increase as Ag/Au in the initial system decreases (Figs. 2, b–d and 3, e, f). Fine (<5 μm) Au–Ag alloy grains are concentrated in the pyrite mainly along its boundary with pyrrhotite (Figs. 2, b–f and 3, d–f). The pyrite core contains both fine and large (up to 30 μm) rounded
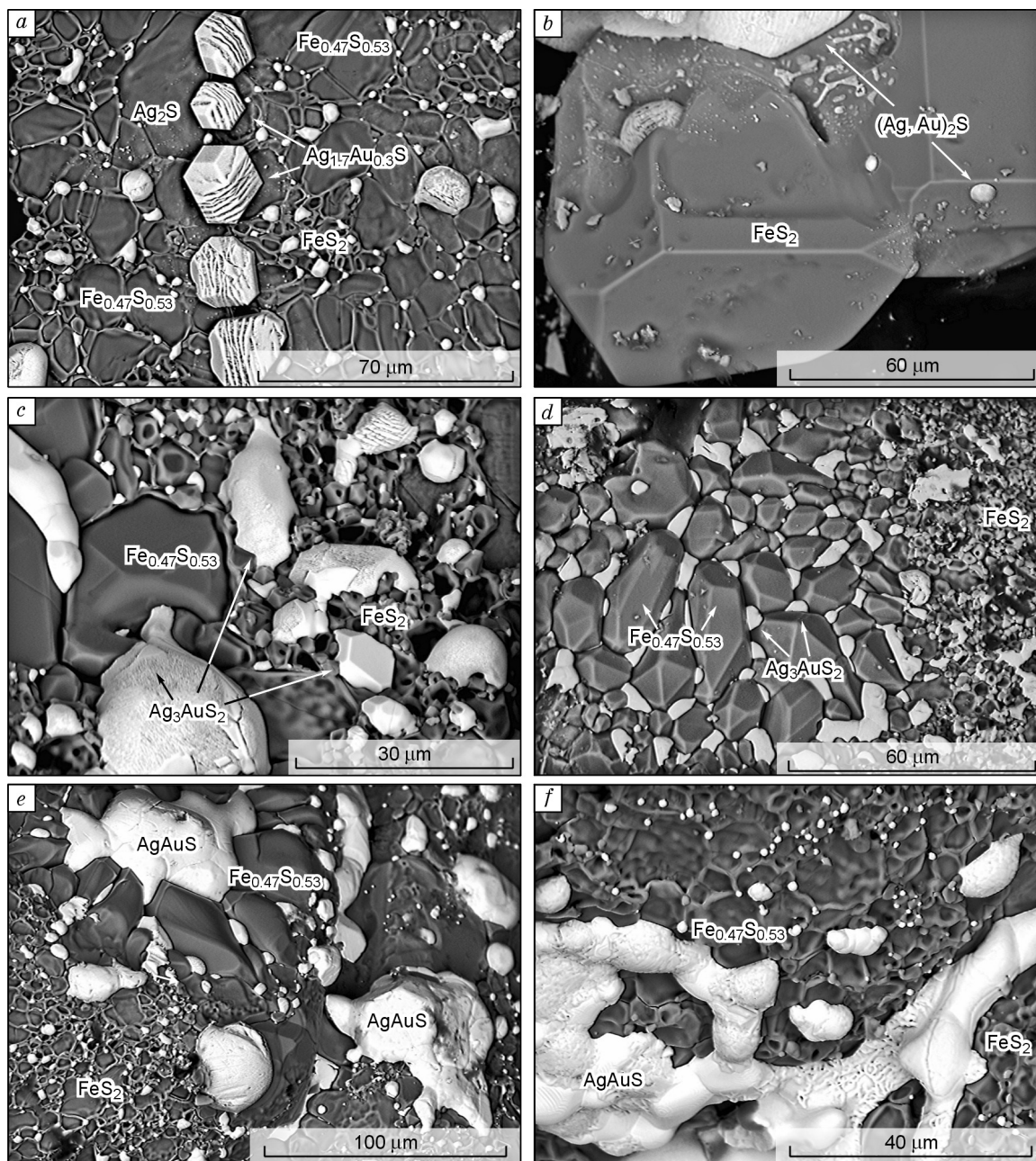
Fig. 4. Reflected-electron photos of aggregates of iron and gold–silver sulfide crystals on the surface of synthesized samples. *a–f*, See Photo 3.

grains of Au–Ag alloys, often intergrown with Au–Ag sulfides (Figs. 2, *e*, *f* and 3, *e*, *f*). The iron content in the large alloy grains does not exceed 5.7 wt.%. The fineness of gold containing Fe impurities (N_{Au} = Au/(Au + Ag + Fe) · 1000‰) increases from 750‰ in experiment 2 to 920–930‰ in experiments 3 and 4.

The composition of Au–Ag sulfides depends first of all on the initial Ag/Au ratios in experimental samples (Table 1). In experiment 1, silver sulfide is close in stoichiometric composition to acanthite (Ag/Au = 10). Solid solutions of Au–Ag sulfides were found in experiments 1 and 2: $Ag_{1.6}Au_{0.2}Fe_{0.1}S_{1.1}$ and $Ag_{1.3}Au_{0.5}Fe_{0.1}S_{1.2}$, respectively. In experiments 2 and 3, the obtained Au–Ag sulfides are similar in composition to uytenbogaardtite. In experiments 3 and 4,

the Au–Ag sulfides are close (within the analytical error) to the stoichiometric composition of petrovskaite. Gold–silver sulfides contain iron impurities, whose concentration does not exceed 3.3 wt.%. Figures 4, *a–f* and 5, *b* show Au–Ag sulfide microcrystals found on the surface of experimental solid products. Most often, they are rounded (Fig. 4, *b–f*) and are localized between pyrite or, seldom, pyrrhotite grains. Well-faceted crystals of Au–Ag sulfides (Fig. 4, *a*, *c*) were produced in the experiments with the highest initial Ag/Au ratios (≥2). These are, most likely, paramorphs of low-temperature modifications on high-temperature ones. In all experiments, there are minor amounts of elemental sulfur on the surface of solid phases or the ampoule walls.

X-ray diffraction spectral data

The X-ray diffraction spectral analysis showed that all studied samples contain pyrite FeS_2 (The Powder Diffraction..., 2006, card 04-004-6511) and monoclinic pyrrhotite Fe_7S_8 (card 00-029-0723). The sample from experiment 1 also contains acanthite (card 004-008-8450). The diffraction pattern of the sample from experiment 2 has weak diffusive peaks assigned to uytenbogaardtite (card 00-020-0461). The samples from experiments 3 and 4 contain petrovskaite (card 00-019-1146) and metallic phase, whose peaks are similar to those of silver (card 04-007-7997), gold (card 04-007-8000), and their alloys. A metallic phase is also present in a minor amount in experiment 3 and in a much greater amount in experiment 4, whereas petrovskaite is more abundant in experiment 3. The weak peaks on the diffraction patterns of all samples are assigned to sulfur.

Discussion

The experimental results for the studied system Fe–Ag–Au–S were interpreted using available data on binary and ternary subsystems and the melting points of possible solid phases (Barnes, 1997; Barton, 1980; Taylor, 1970a,b; Vaughan and Craig, 1978; Vol and Kogan, 1976; Waldner and Pelton, 2005). For example, the melting point of hexagonal pyrrhotite is 1195 ℃. But in the S-enriched (>50 at.% S) system Fe–S, including the initial composition specified in our experiments (33.33 at.% Fe and 66.66 at.% S; Ag and Au are ignored), its melting point decreases to ~1100 ℃ (Waldner and Pelton, 2005). In the ternary system Ag–Au–S, an Au–Ag–S melt is produced at >700–840 ℃; its composition is determined by the proportion of elements (Barton, 1980). In the Ag-rich systems, cooling of Ag-rich melts results in solid solutions of Au–Ag sulfides, $Ag_{2-x}S$ $(x \to 0)$–$Au_{0.1}Ag_{1.9}S$ and $Au_{0.1}Ag_{1.9}S$–$Au_{0.4}Ag_{1.6}S$, with face- and space-centered lattices, respectively. In the Au-rich systems, high-fineness gold and a solid solution of Au–Ag sulfides with a primitive cubic lattice are produced.

By analogy to the systems Pb–Ag–FeS and Pb–Au–FeS (Raghavan, 2009; Rybkin et al., 2006), we suggest that the system under study includes immiscible liquids—iron sulfide melt with impurities of noble metals, L_1 (Fe,S ≫ Ag > Au), and gold–silver sulfide melt with iron impurities, L_2 (Ag,Au,S ≫ Fe). In accordance with the Fe–S diagram (Fig. 1, a), the specified composition falls in the liquation domain involving liquid sulfur. This suggests the presence of the third phase, L_S, in the system. On cooling, the melt L_1 produces hexagonal pyrrhotite (Fig. 1, a). Noble metals dissolved in L_1 crystallize at the final stage, yielding xenomorphic fine grains of native gold and Au–Ag sulfides (Fig. 2, a–e). Further cooling leads to the production of pyrite by the peritectic reaction $FeS + L_S = FeS_2$ (Fig. 1, a). This is confirmed by the resorbed surface of pyrrhotite in all experiments and the euhedral pyrite grains growing over the larger pyrrhotite grains (Figs. 2, a–d and 3, b–f). As a result,
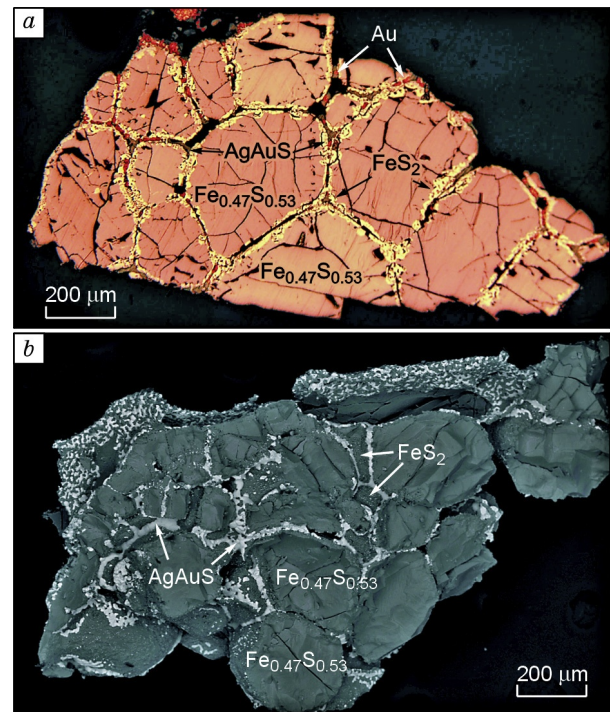

Fig. 5. Inequigranular texture of synthesized sample (experiment 4) with coarse euhedral pyrrhotite grains, with fine-grained aggregates of pyrite, petrovskaite, and high-fineness gold between them. a, Reflected-light photo, nicols ×; b, reflected-electron photo.

microinclusions of native gold and Au–Ag sulfides get into the pyrite grains and are arranged parallel to the pyrite/pyrrhotite boundary. The large and fine rounded grains of Fe-containing gold (Fig. 2, b–d) and Au–Ag sulfides (Figs. 2, a–e and 3, a–f) forming emulsion-like impregnations in the pyrite grain cores are the exsolution products of solid solutions crystallized from the melt L_2 (Au,Ag,S > Fe). At 317 and 113 ℃, hexagonal pyrrhotite passes into a monoclinic one, and liquid sulfur passes into a solid one (Fig. 1, a). Sulfur is present as drops on the ampoule walls and on the sample surface is the last solid phase. Transition of high-temperature polymorphic Au–Ag sulfides into low-temperature ones ($\alpha \to \beta$) occurs in the temperature range 177–307 ℃ (Barton, 1980). Annealing at 150 ℃ leads to the ordering of the structure of low-temperature polymorphic Au–Ag sulfides and the formation of microcrystals on the sample surface (Fig. 4, a–f).

Thus, the experimental results show the possible crystallization of Au–Ag sulfides from melts $FeAg_{0.1-0.1x}Au_{g0.1x}S_2$. The Ag-rich systems (Ag/Au > 2) lack native gold. As the content of gold in the system Fe–Ag–Au–S increases, only high-fineness gold (>750‰) crystallizes. Most of the Au–Ag phases are produced from the Au–Ag sulfide melt L_2 (Au,Ag,S > Fe), which exists autonomously from the iron sulfide melt L_1 (Fe,S ≫ Ag > Au). These phases crystallize at the intermediate stages of sulfide melt evolution after pyrrhotite but before pyrite. The experimental results account for the low contents of Au and Ag in the pyrrhotites of sulfide ores from the Noril'sk district (Barnes et al., 2006; Sluzhenikin

and Mokhov, 2002) and suggest high gold and silver contents in pyrite ores. These data also confirm the model of fractional crystallization of sulfide melts with the formation of noble-metal mineral phases (Ebel and Naldrett, 1996, 1997; Sinyakova et al., 2006). In natural ore-forming processes, crystallization of sulfide melts can yield Au–Ag sulfides and high-fineness gold. Judging from the clarke ratios Ag/Au > 10, Au–Ag sulfides will be predominant species of these metals. We think Au–Ag sulfides can be of wider occurrence and be present in almost all pyrite ores of deposits of different genesis.

Conclusions

1. Depending on Ag/Au in the system FeS_2–Ag–Au, Au–Ag sulfides of different compositions with up to 3.3 wt.% Fe are produced.

2. In the Au-rich systems, Au–Ag sulfides along with high-fineness gold are formed. The minimum fineness of native gold produced during the crystallization of Au–Ag sulfide melt is 750‰ (with regard to the presence of up to 5.7 wt.% Fe).

3. At 1050 ºC, both iron sulfide melt with impurities of noble metals (Fe,S,Ag ≫ Au) and Au–Ag sulfide melt with Fe impurities (Au,Ag,S ≫ Fe) exist. On cooling of the melts, a successive crystallization of pyrrhotite, high-fineness gold (at Ag/Au ≥ 2), Au–Ag sulfides (micro- and macrograins), pyrite, and sulfur occurs.

4. Gold–silver sulfides are stable and dominate over native metals, especially in pyrite ores with high Ag/Au ratios.

References

Barnes, H.L., 1997. Geochemistry of Hydrothermal Ore Deposits, third ed. John Wiley & Sons, New York.

Barnes, S.-J., Cox, R.A., Zientek, M.L., 2006. Platinum-group element, gold, silver and base metal distribution in compositionally zoned sulfide droplets from the Medvezhy Creek Mine, Noril'sk, Russia. Contrib. Mineral. Petrol. 152, 187–200.

Barton, M.D., 1980. The Ag–Au–S system. Econ. Geol. 75, 303–316.

Barton, M.D., Kieft, C., Burke, E.A.J., Oen, I.S., 1978. Uytenbogaardtite, a new silver–gold sulfide. Can. Mineral. 16, 651–657.

Castor, S.B., Sjoberg, J.J., 1993. Uytenbogaardtite, Ag_3AuS_2, in the Bullford mining district, Nevada. Can. Mineral. 31, 89–98.

Chareev, D.A., 2006. Thermodynamics of Pyrite–Pyrrhotite Equilibrium at 500–730 K and 1–5000 bars in the System Ag–Fe–S and PT-Conditions of Formation of Metallic Silver. PhD Thesis [in Russian]. IEM RAN, Chernogolovka.

Cook, N.J., Chryssoulis, Sl., 1990. Concentrations of 'invisible gold' in the common sulfides. Can. Mineral. 28, 1–16.

Czamanske, G.K., Kunilov, V.E., Zientek, M.L., Cabri, L.J., Likhachev, A.P., Calk, L.C., Oscarson, R.L., 1992. A proton-microprobe study of magmatic sulfide ores from the Noril'sk–Talnakh district, Siberia. Can. Mineral. 30, 249–287.

Ebel, D.S., Naldrett, A.J., 1996. Fractional crystallization of sulfide ore liquids at high temperature. Econ. Geol. 91, 607–621.

Ebel, D.S., Naldrett, A.J., 1997. Crystallization of sulfide liquids and the interpretation of ore composition. Can. J. Earth Sci. 34, 352–365.

Geiger, T., Bischoff, A., 1995. Formation of opaque minerals in CK chondrites. Planet. Space Sci. 43 (3–4), 485–498.

Mironov, A.G., Tauson, V.L., Geletii, V.F., 1987. A metal bond as a factor favoring the incorporation of gold into sulfide mineral structures. Dokl. Akad. Nauk 293 (2), 447–449.

Mungall, J.E., Andrews, D.R.A., Cabri, L.J., Sylvester, P.J., Tubrett, M., 2005. Partitioning of Cu, Ni, Au, and platinum-group elements between monosulfide solid solution and sulfide melt under controlled oxygen and sulfur fugacities. Geochim. Cosmochim. Acta 69, 4349–4360.

Nadeau, O., Williams-Jones, A., Stix, J., 2010. Sulphide magma as a source of metals in arc-related magmatic hydrothermal ore fluids. Nat. Geosci. 3, 501–505.

Nesterenko, G.V., Kuznetsova, A.P., Pal'chik, N.A., Lavrent'ev, Yu.G., 1984. Petrovskaite AuAg(S,Se), a new Se-containing Au–Ag sulfide. Zapiski VMO, No. 5, 602–607.

Osadchii, E.G., Rappo, O.A., 2004. Determination of standard thermodynamic properties of sulfides in the Ag–Au–S system by means of a solid-state galvanic cell. Am. Mineral. 89, 1405–1410.

Pal'yanova, G.A., Savva, N.E., 2007. Genesis of Au–Ag sulfides at the Ulakhan deposit (Russia), in: Bullen, T., Wang, Y. (Eds.), Proc. 12th Int. Symp. Water–Rock Interaction. China, Kunming, Vol. 1, pp. 377–380.

Pal'yanova, G.A., Savva, N.E., 2009. Specific genesis of gold and silver sulfides at the Yunoe deposit (Magadan Region, Russia). Russian Geology and Geophysics (Geologiya i Geofizika) 50 (7), 587–602 (759–777).

Pal'yanova, G.A., Kokh, K.A., Yu.V. Seryotkin, 2011a. Formation of gold and silver sulfides in the system Ag–Au–S. Russian Geology and Geophysics (Geologiya i Geofizika) 52 (4), 443–449 (568–575).

Pal'yanova, G.A., Yu.V. Seryotkin, Kokh, K.A., 2011b. Formation of gold and silver sulfides from melts in the Ag–Au–S system: experimental data. Dokl. Earth Sci. 436 (1), 42–46.

Pal'yanova, G.A., Savva, N.E., Okrugin, V.M., 2011c. Genesis of gold–silver sulfides and selenides at deposits in northeastern Russia, in: Abstr. Second Int. Mining and Geological Forum "Gold of the Northern Pacific Periphery", Magadan, 3–5 September 2011 [in Russian]. NEIRI FEB RAS, Magadan, pp. 33–35.

Raghavan, V., 2009. Au–Fe–Pb–S (gold–iron–lead–sulphur). J. Phase Equilibria and Diffusion 30 (1), 111.

Ryabchikov, I.D., Orlova, G.P., Babanskii, A.D., Magazina, L.O., Tsepin, A.I., 1999. Chalcophile metals in the processes of the mantle magma and Earth's core formation. Rossiskii Zhurnal Nauk o Zemle 1 (6), http://elpub.wdcb.ru/journals/rjes/rus/v01/rje99023.htm#chap00.

Rybkin, S.G., Nikolaev, Yu.L., Barankevich, V.G., 2006. Isothermal sections of the Pb–Au–FeS and Pb–Ag–FeS diagrams at 1473 K. Zhurnal Neorganicheskoi Khimii 51 (3), 470–473.

Savva, N.E., Pal'yanova, G.A., 2007. Genesis of gold and silver sulfides at the Ulakhan deposit (northeastern Russia). Russian Geology and Geophysics (Geologiya i Geofizika) 48 (10), 799–810 (1028–1041).

Savva, N.E., Pal'yanova, G.A., Byankin, M.A., 2010a. A possible mechanism of the formation of uytenbogaardtite and fischesserite at the Kupol deposit, in: Proc. All-Russian Conf. "Native Gold: Typomorphism of Mineral Assemblages, Formation Conditions of Deposits, and Problems of Applied Research" [in Russian]. IGEM RAN, Moscow, Vol. 2, pp. 173–175.

Savva, N.E., Pal'yanova, G.A., Kozlova, E.E., 2010b. Gold and silver minerals in zone of secondary sulfide enrichment (Krutoe ore occurrence, northeastern Russia). Vestnik SVNTs DVO RAN, No. 1, 33–45.

Sazonov, A.M., Zvyagina, E.A., Leont'ev, S.I., Vul'f, M.V., Poleva, T.V., Chekushin, V.S., Oleinikova, N.V., 2008. Associations of micro- and nanosized segregations of noble metals in ores. Zhurnal Sibirskogo Federal'nogo Universiteta. Ser. Tekhnika i Tekhnologiya, No. 1, 17–32.

Sinyakova, E.F., Kosyakov, V.I., Pavlyuchenko, V.S., 2006. The behavior of ore components during directed crystallization of melt close in composition to natural magmatic Fe–Cu–Ni–S liquid, with impurities of Pt, Pd, Rh, Ru, Ir, Au, Ag, and Co. Vestnik Otdeleniya Nauk o Zemle RAN, No. 1 (24), http://www.scgis.ru/russian/cp1251/h_dgggms/1-2006/inform-bul-1_2006/term-46.pdf.

Sluzhenikin, S.F., Mokhov, A.V., 2002. Gold and silver in deposits of the Noril'sk district, in: Proc. All-Russian Symp. "Geology, Genesis, and Problems of Exploration of Complex Noble-Metal Deposits" [in Russian]. IGEM RAN, Moscow, pp. 326–330.

Sluzhenikin, S.F., Mokhov, A.V., 2010. Gold and silver in Pt-Cu-Ni- and Pt-ores of the Noril'sk district: distribution and species, in: Proc. All-Russian Conf. "Native Gold: Typomorphism of Mineral Assemblages, Formation Conditions of Deposits, and Problems of Applied Research" [in Russian]. IGEM RAN, Moscow, Vol. 2, pp. 212–214.

Spiridonov, E.M., 2010a. Minerals of the Au–Ag series of the Noril'sk sulfide ores, in: Proc. All-Russian Conf. "Native Gold: Typomorphism of Mineral Assemblages, Formation Conditions of Deposits, and Problems of Applied Research" [in Russian]. IGEM RAN, Moscow, Vol. 2, pp. 229–232.

Spiridonov, E.M., 2010b. Review of gold minerals in the main types of gold mineralization, in: Gold of the Kola Peninsula and Adjacent Regions. Proc. All-Russian (with International Participation) Sci. Conf. Dedicated to the 80th Anniversary of the Kola Scientific Center, Apatity, 26–29 September 2010 [in Russian]. Izd. K & M, Apatity, pp. 143–171.

Tauson, V.L., Mironov, A.G., Smagunov, N.V., Bugaeva, B.G., Akimov, V.V., 1996. Gold in sulfides: state of the art of occurrence and horizons of experimental studies. Geologiya i Geofizika (Russian Geology and Geophysics) 37 (3), 3–14 (1–11).

Tauson, V.L., Pastushkova, T.M., Bessarabova, O.I., 1998. On limit concentration and manner of incoroporation of gold in hydrothermal pyrite. Geologiya i Geofizika (Russian Geology and Geophysics) 39 (7), 924–933 (932–940).

Tauson, V.L., Smagunov, N.V., Pastushkova, T.M., 2005. Incorporation of gold into pyrrhotite and the influence of nonautonomous phases on its distribution. Geokhimiya, No. 1, 96–100.

Taylor, L.A., 1970a. The system Ag–Fe–S: phase equilibria and mineral assemblages. Mineral. Depos. 5, 41–58.

Taylor, L.A., 1970b. The system Ag–Fe–S: phase relations between 1200 and 700 ºC. Metall. Trans. 1, 2523–2529.

The Powder Diffraction File PDF-4+, International Centre for Diffraction Data (ICDD), Release 2006.

Vaughan, D.J., Craig, J.R., 1978. Mineral Chemistry of Metal Sulfides. Cambridge University Press, Cambridge.

Vol, A.E., Kogan, I.K., 1976. The Structure and Properties of Binary Metal Systems [in Russian]. Nauka, Moscow.

Wager, L.R., Brown, G.M., 1968. Layered Igneous Complexes. Oliver and Boyd, Edinburgh.

Waldner, P., Pelton, A.D., 2005. Thermodynamic modeling of the Fe–S system. J. Phase Equilibria and Diffusion 26 (1), 23–38.

Editorial responsibility: A.S. Borisenko